The Journal of Chemical Physics

Evidence of supercoolable nanoscale water clusters in an amorphous ionic liquid matrix

Cite as: J. Chem. Phys. **155**, 174501 (2021); https://doi.org/10.1063/5.0066180
Submitted: 09 August 2021 • Accepted: 08 October 2021 • Published Online: 01 November 2021

Florian Pabst, Jennifer Kraus, Sebastian Kloth, et al.

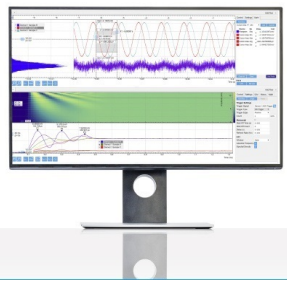

The Journal of Chemical Physics ARTICLE scitation.org/journal/jcp

Evidence of supercoolable nanoscale water clusters in an amorphous ionic liquid matrix

Cite as: J. Chem. Phys. 155, 174501 (2021); doi: 10.1063/5.0066180
Submitted: 9 August 2021 • Accepted: 8 October 2021 •
Published Online: 1 November 2021

Florian Pabst,[1,a)] Jennifer Kraus,[1] Sebastian Kloth,[1] Elisa Steinrücken,[1] Margarita Kruteva,[2] Aurel Radulescu,[3] Michael Vogel,[1] and Thomas Blochowicz[1,b)]

AFFILIATIONS

[1] TU Darmstadt, Institute for Condensed Matter Physics, 64289 Darmstadt, Germany
[2] Jülich Centre for Neutron Science JCNS (JCNS-1), Forschungszentrum Jülich GmbH, 52425 Jülich, Germany
[3] Jülich Centre for Neutron Science (JCNS) at Heinz Maier-Leibnitz Zentrum (MLZ), Forschungszentrum Jülich GmbH, 85747 Garching, Germany

[a)] **Author to whom correspondence should be addressed:** fpabst@fkp.tu-darmstadt.de
[b)] thomas.blochowicz@physik.tu-darmstadt.de

ABSTRACT

Nanoscale water clusters in an ionic liquid matrix, also called "water pockets," were previously found in some mixtures of water with ionic liquids containing hydrophilic anions. However, in these systems, at least partial crystallization occurs upon supercooling. In this work, we show for mixtures of 1-butyl-3-methylimidazolium dicyanamide with water that none of the components crystallizes up to a water content of 72 mol. %. The dynamics of the ionic liquid matrix is monitored from above room temperature down to the glass transition by combining depolarized dynamic light scattering with broadband dielectric and nuclear magnetic resonance spectroscopy, revealing that the matrix behaves like a common glass former and stays amorphous in the whole temperature range. Moreover, we demonstrate by a combination of Raman spectroscopy, small angle neutron scattering, and molecular dynamics simulation that, indeed, nanoscale water clusters exist in this mixture.

I. INTRODUCTION

When studying ionic liquids (ILs) experimentally, it is inevitable to consider water as an additive. This is because ILs are often hydrophilic, so an uptake of water from air can lead to not only a dramatic change in physicochemical properties, such as viscosity[1] or glass transition temperature,[2] i.e., it affects the molecular dynamics (MD), but also differences in the crystallization behavior of the liquid.[3] Therefore, ILs are usually dried in a vacuum oven before characterization to ensure the absence of water. Conversely, intentionally added water can alter the properties of the IL in a desired direction, for example, to enhance the conductivity.[4]

Another interesting observation was made when adding a certain amount of water to some hydrophilic ILs: In a narrow composition range, nanoscale water clusters, also called *water pockets*, were shown to form in the ionic liquid matrix. This was experimentally observed by small angle neutron scattering (SANS),[5,6] Raman spectroscopy,[7,8] and nuclear magnetic resonance (NMR) measurements.[9] These findings were supported by molecular dynamics simulations,[10,11] where water pockets were also identified. Because of the balanced interplay between Coulomb forces and H bonds needed for water pockets to form, it is intriguing to study the formation of these structures in an ionic liquid, which often shows nanostructuration itself due to the ordering of polar and apolar domains.[12] However, confined water by itself is a large area of research; see, for example, Ref. 13 and references therein. One aspect of this research field is that in confinement it is possible to access supercooled water at all temperatures without intervening crystallization, while bulk water inevitably crystallizes in a certain temperature range, the so-called "no man's land." Thus, water pockets could be used to study supercooled nanoscale water clusters in an IL matrix. One requirement is, of course, that the water pockets do not crystallize. Furthermore, we also require the IL to be easily supercooled in order to access the dynamics of the mixture with optical methods, like intended in this work. These premises exclude the two

most studied ILs with respect to water pocket formation, namely, 1-butyl-3-methylimidazolium tetrafluoroboarate ([BMIM][BF_4]) and 1-butyl-3-methylimidazolium nitrate ([BMIM][NO_3]), where the crystallization of at least one component was reported.[14,15]

Therefore, the aim of this work is to find an IL, which in mixtures with water allows for the formation of water pockets without crystallization of neither component on supercooling. We choose 1-butyl-3-methylimidazolium dicyanamide ([BMIM][DCA]) because it is known that it is miscible with water due to the hydrophilic anion[16] and is easily supercooled in the neat form.[17]

II. METHODS

The IL 1-butyl-3-methylimidazolium dicyanamide ([BMIM][DCA]) was purchased from Iolitec GmbH with a specified purity of >98%, and the chemical structure of the constituents is depicted in Fig. 1. The IL was dried for at least 24 h before use. Deuterated water was purchased from Deutero GmbH with a purity of 99.9%, and deionized water was taken from a Milli-Q water purification system. Mixtures were prepared by weighing, and the concentrations are given in mol. % with an error not exceeding ±1%. For light scattering measurements, all components were filtered before mixing using a syringe filter with a pore size of 200 nm to reduce dust.

For small angle neutron scattering (SANS) and NMR diffusion measurements, the cations were deuterated at the C2 position of the imidazolium ring,[18–20] i.e., the position between the two nitrogen atoms, utilizing deuterated water. This is necessary to suppress the chemical exchange between protons/deuterons of water and cations at the C2 position. After drying, the degree of deuteration of the IL that was used for SANS was 91% as probed by ^{1}H NMR spectra, while it was only 60% in the case of the IL used for NMR diffusion measurements. Still, the latter deuteration degree is sufficient for the NMR diffusion measurements because in the resulting mixture with D_2O, 98% of the ^{1}H nuclei were located at cations and only 2% were at water molecules, allowing us to probe cation diffusion via ^{1}H NMR in the mixture. For the IL with a deuteration degree of 91% for the SANS measurements, this ratio results in 99.5% of ^{1}H nuclei at cations and only 0.5% at water molecules. After mixing with D_2O, all NMR samples were immediately sealed in glass tubes. Samples for SANS measurements were contained in Hellma cuvettes with a sample thickness of 1 mm.

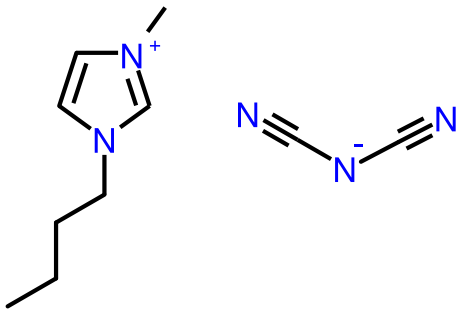

FIG. 1. Ionic liquid 1-butyl-3-methylimidazolium dicyanamide ([BMIM][DCA]).

A. Differential scanning calorimetry

A Perkin Elmer 8000 DSC equipped with a liquid nitrogen cooling system was used for differential scanning calorimetry (DSC) measurements utilizing hermetic sealed sample pans from TA-Instruments. The heat flow of the samples in comparison with an empty sample pan was measured from room temperature down to well below the glass transition and back to room temperature. Heating and cooling rates were identical for each run.

B. Small angle neutron scattering

Small angle neutron measurements were performed by means of the instrument KWS-2 operated by the JCNS at the Heinz Maier-Leibnitz Zentrum (MLZ), Garching, Germany. Detector distances of 1.5 and 4 m were used to cover the scattering vector range from ~0.03 to 1 Å^{-1}. The background from an empty cuvette and dark counts are subtracted from all the data. The measurements were carried out at 25 and 5 °C.

C. Raman spectroscopy

Polarized Raman spectra were measured with a Jobin Yvon U1000 double monochromator in the backscattering geometry using a Cobolt Samba laser with a wavelength of 532 nm and a power of 10 mW. The resolution set by the entrance and exit slits was ~5 cm^{-1}, as determined by the FWHM of the laser line. The scattered light was detected by using a Hamamatsu photomultiplier tube and recorded with a LabView program.

D. Dynamic light scattering

Photon correlation spectroscopy (PCS) experiments were performed using a Cobolt Samba laser (λ = 532 nm) operated at 100 mW. The sample was mounted in a Cryovac cold-finger cryostat that gives access to a temperature range from 77 to 400 K. The scattered light was collected into a single-mode optical fiber and fed over a beam splitter into two Laser Components COUNT T100 avalanche photodiodes. The time dependent scattered intensity was recorded with an ALV 7000 hardware correlator in the quasi-cross correlation mode in order to suppress afterpulsing. The detection optics were mounted at 90° to the incident beam. The polarization of the incident beam and the scattered light was selected by means of two polarizers from Bernhard Halle to be vertical–horizontal (VH).

Tandem Fabry–Pérot interferometry (TFPI) measurements were performed with a Sandercock triple pass interferometer in backscattering geometry and a Coherent Verdi V2 Laser (λ = 532 nm) operating between 200 and 400 mW. The sample was mounted in a home-built oven.

E. Dielectric spectroscopy

Broadband dielectric spectroscopy (BDS) was carried out in the frequency range from 1×10^{-2} to 1×10^{7} Hz with a Novocontrol Alpha-N high resolution dielectric analyzer, where temperature was controlled utilizing a Novocontrol Quatro cryosystem. A custom made sample cell, which consisted of two polished stainless steel electrodes spaced by a quartz glass ring, providing a sample thickness of ~400 μm, was used for dynamical measurements due to its low electrode polarization. For conductivity measurements, another

TABLE I. Number of ion pairs N_{pairs}, number of water molecules N_W, and length L of the cubic simulation boxes for each water concentration in the MD simulation.

Mol. %	N_{pairs}	N_W	L (nm)
0	350	0	4.85
50	350	350	5.01
72	350	900	5.22
80	350	1400	5.40
88	350	2567	5.78

custom made sample cell was used, which can be sealed air-tight and which is better suited for accurate calibration.

F. Nuclear magnetic resonance

^{1}H NMR diffusion measurements were carried out with a specifically designed static field gradient (SFG) setup, which features super-conducting coils in the anti-Helmholtz arrangement to produce a magnetic field with very high static gradients.[21] The sample was placed at a position where the ^{1}H Larmor frequency amounts to $2\pi \cdot 92.0$ MHz and the field gradient is $g = 179$ T/m. The 90° pulse length was about 1 μs. Temperature was controlled by using a passive cooling cryostat, stabilizing the temperature to ±0.1 K.

G. Molecular dynamics simulation

All MD simulations were performed at 300 K under periodic boundary conditions using the GROMACS 2018.3 software.[22,23] To adjust the density, equilibration runs in the *NpT* ensemble at a pressure of $p = 1$ bar preceded the production runs (200 ns) in the canonical *NVT* ensemble. The Parinello–Rahman barostat and the velocity-rescale thermostat[24] with a time constant of 1 ps were employed to set the pressure p and temperature T, respectively.

For [BMIM][DCA], we used the interaction potential proposed by Doherty *et al.*[25] This all-atom model has reduced ionic charges of ±0.8e to account for polarization effects. For water, we used the water model TIP4P/2005 from the work of Abascal and Vega.[26]

Each system contains 350 ion pairs, and water was added to adjust the desired concentration (see Table I), resulting in box lengths L of ~5 nm. To compute the long-range part of electrostatic and Lennard-Jones interactions, the particle mesh Ewald (PME) method[27] was utilized with a direct space cutoff of 1.3 nm and a Fourier grid spacing of 0.15 nm.

III. RESULTS

A. Differential scanning calorimetry

We performed calorimetric temperature scans for several water concentrations from pure IL up to 88 mol. % water with slow cooling and heating rates of 2.5 K/min to see if crystallization occurs in these samples. For water concentrations of up to 72 mol. %, a glass transition step is visible, which shifts to lower temperature with increasing water concentration, see Fig. 2, where heating curves for different amounts of water are shown. Moreover, no peak due to crystallization/melting shows up for this range of water concentrations.

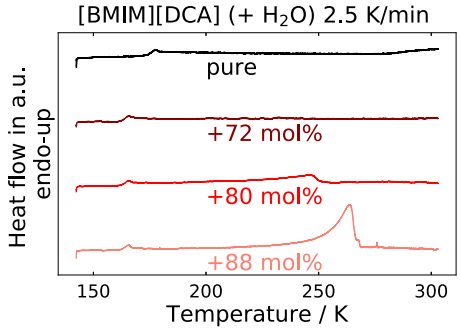

FIG. 2. Heat flow curves obtained with a cooling and heating rate of 2.5 K/min for mixtures as indicated. A glass transition step is visible for all concentrations; a melting peak only shows up for water concentrations above 72 mol. %.

For water concentrations of 80 and 88 mol. %, an endothermic peak is visible in the heat flow curves, indicating melting of formerly crystallized parts of the sample, presumably water. The glass transition step, however, is still visible and located at approximately the same temperature as in the 72 mol. % sample, indicating that the IL together with some portion of the water undergoes a joint glass transition, while excess water freezes.

Additionally, for the neat IL and the mixture with 72 mol. % water, measurements were performed with 5, 10, 20, 40, and 80 K/min, from which calorimetric relaxation times were extracted by fitting the glass transition step with the Tool–Naranayaswamy–Moynihan–Hodge (TNMH) model. The details of this procedure are omitted here for sake of brevity but can be found in Ref. 28. The obtained relaxation times will be discussed below.

B. Raman spectroscopy

Raman spectroscopy is a versatile tool for the investigation of molecular vibrational modes. Of special interest in this work are the OH stretching bands of water because it has been shown that different OH vibrations can be assigned to OH groups, which are involved in different hydrogen-bonded structures.[29] In this respect, the so-called fully bonded water with two donor (D) and two acceptor (A) bonds per molecule can be regarded as evidence for the presence of larger water clusters because this type of bonding cannot occur in small water clusters. This fact was exploited previously to prove the existence of water pockets in an IL matrix.[7]

Our measurements of neat water are shown in Fig. 3, including a fit with five Gaussian subbands, assigned according to Ref. 29 to differently bonded water molecules. A sketch of the different bonding types is included in Fig. 3.

It is evident that the *DDAA* band is very prominent in bulk water due to fully bonded water molecules in the hydrogen-bonding network. To check whether this band is also present in the IL–water mixtures and indicates the presence of water pockets, we show Raman spectra of several water concentrations between 0 and 88 mol. % water in Fig. 4. Since the IL shows fluorescence when illuminated with green light, we fitted a broad background Gaussian peak at around 1500 cm^{-1} to each spectrum and subtracted this background from the data before further evaluation. Then, all

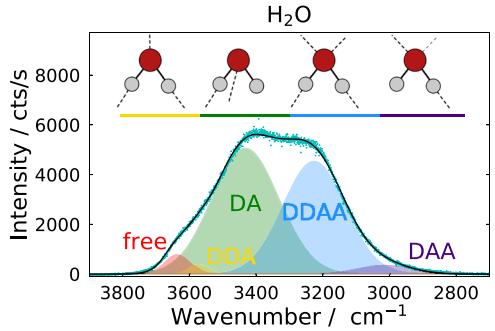

FIG. 3. Raman spectrum of neat water at room temperature in the OH stretching region. The solid line represents the overall fit comprised of the subbands depicted as shaded areas and assigned to the differently bonded water molecules, as shown by the sketches above the data, according to Ref. 29.

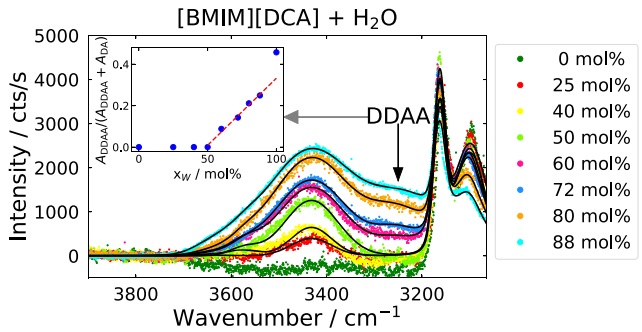

FIG. 4. Raman spectra in the OH stretching region for mixtures of IL with water as indicated. The *DDAA* subband, as an evidence of fully bonded water, only shows up for concentrations starting from 60 mol. % water. Inset: Ratio of the areas of the *DDAA* peak to the sum of *DA* and *DDAA* area.

spectra were described with the same subbands in the OH stretching region as for neat water and additionally with subbands accounting for the CH stretching vibrations of the cation.[30] The weak *DAA* peak was omitted in the mixtures due to the overlap with the CH stretching bands.

As can be seen, up to a water concentration of 50 mol. %, no *DDAA* peak appears in the spectra within experimental uncertainty. Instead, only the *DA* contribution increases in intensity with increasing amount of water. For higher concentrations, however, besides the *DA* peak increasing further in intensity, a clear additional peak arises in the wavenumber region of the *DDAA* signature. In the inset of Fig. 4, the area of the *DDAA* peak in relation to the total area of the *DA* plus *DDAA* peaks is shown for all water concentrations. The reason for choosing this representation instead of focusing on the absolute intensity of the *DDAA* peak is that the area ratio of the two peaks is basically unaffected by inaccuracies of the background subtraction or by intensity variations inherent to the long duration of the measurement series. The fit parameters of all subbands are shown in Fig. 12 in the Appendix. As can be seen in the inset of Fig. 4, the intensity of the *DDAA* peak increases linearly with respect to the intensity of the *DA* peak from 60 mol. % on. We note that this linear dependence does not extrapolate to the measured value of pure water, which might be a hint of some anions taking part in the hydrogen-bonding network in the mixtures, reducing the number of fully bonded water molecules. This is, most probably, also the reason for the *DDAA* peak being red shifted by ~30 cm^{-1} in the 60 mol. % mixture with respect to neat water. This red shift continuously decreases upon the addition of water. The notion of anions being responsible for this behavior is supported when considering the C–N stretching vibration of the anion at around 2190 cm^{-1}[31] (see Fig. 13 in the Appendix): The frequency of this vibration is shifted toward higher wavenumbers upon the addition of water, accompanied by the same behavior of the C–H stretching vibration of the C2 atom around 3116 cm^{-1},[30] as can be seen on the far right in Fig. 4. This blue shift indicates a stronger C–N bond of the anion and analogously a stronger C2–H bond of the cation, which can be seen as a loss of the cation–anion interaction C2–H ···N with increasing water content. The ion-pair interactions are replaced by H-bond interactions between anion and water, as reported previously for a tetraborate anion containing system.[7]

Together, the appearance of the *DDAA* peak for concentrations starting from 60 mol. % is strong evidence for large water clusters in these mixtures, which are formed by water associated with the anions. However, especially for the highest concentrations, it might be possible that this is not due to nanoscale water clusters but is due to a percolating water network, spanning the whole sample. This will be discussed further below.

C. Dynamic light scattering

In dynamic light scattering (DLS) measurements, reorientational motions of optically anisotropic molecules can be monitored in the vertical–horizontal (VH) polarization mode, i.e., with an analyzer only selecting scattered light polarized perpendicular to the polarization of the incident beam.

In the case of PCS measurements, from the intensity autocorrelation function, the field autocorrelation function $g_1(t)$ is calculated via the Siegert relation for partially heterodyne signals as detailed elsewhere.[32] It is Fourier transformed afterward, combined with TFPI measurements, and all data are described in the frequency domain with a Cole–Davidson (CD) function

$$\chi''(\omega) = \frac{d}{(1 + i\omega\tau_{CD})^{\beta_{CD}}}. \quad (1)$$

Since both the cation and the anion are optically anisotropic, rotational contributions from both ions are expected to be present in the spectra of the neat IL. However, as shown in earlier studies,[18,33] for anions and cations of similar size, the rotations occur on similar timescales. In comparison to the ions, water molecules possess a very small optical anisotropy; thus, contributions from water molecules are most probably not visible in the light scattering spectra. Some spectra of the sample with 72 mol. % water are shown for selected temperatures in Fig. 5, where it can be seen that the fit with one CD function suffices to describe the data in the α-relaxation region, thus confirming the above picture of the ion dynamics being very similar and the water dynamics being either not visible or taking place on a similar timescale, too.

We note that the shape parameter β_{CD} is 0.5 for the mixture with 72 mol. % water at all temperatures, whereas for the neat IL, it is ~0.54, indicating that the heterogeneity of the rotational dynamics increases slightly with the addition of water.

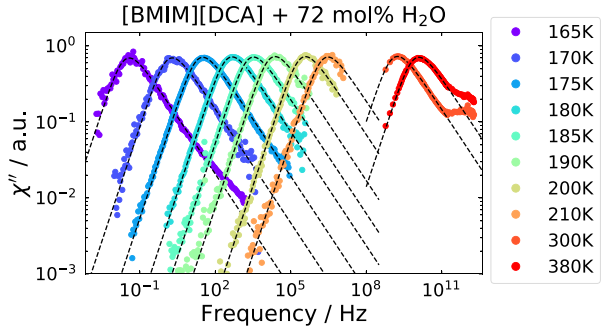

FIG. 5. Dynamic light scattering spectra for selected temperatures. The dashed lines represent fits with a CD function utilizing a stretching exponent of $\beta_{CD} = 0.5$ for the α-process region.

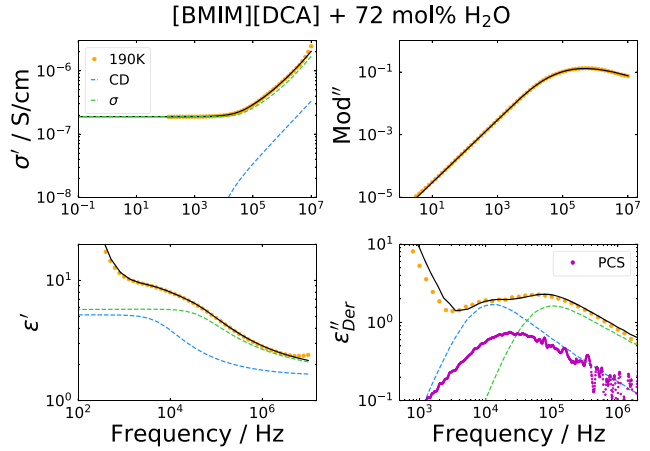

FIG. 6. Dielectric spectra of the mixture with 72 mol. % water in four different representations at 190 K. The black solid line represents the overall fit comprised of a CD function for ion reorientation (blue dashed line) and the MIGRATION model describing the ion hopping relaxation (green dashed line). The light scattering spectrum recorded at the same temperature is added to the ε''_{der} representation.

D. Dielectric spectroscopy

Dielectric spectra were obtained from 250 K down to the glass transition temperature. The data evaluation was performed simultaneously in different representations, i.e., dielectric permittivity $\varepsilon^*(\omega)$, dielectric modulus $M^*(\omega)$, and conductivity $\sigma^*(\omega)$, which are interconnected by

$$\varepsilon^*(\omega) = \frac{1}{M^*(\omega)} = \frac{\sigma^*(\omega)}{i\varepsilon_0\omega} \tag{2}$$

and thus contain the same information. Since the dielectric loss $\varepsilon''(\omega)$ is rather featureless in conducting materials due to the dc-conductivity contribution overshadowing all relaxation processes, it is instructive to use the so-called conductivity free representation of the dielectric loss, which is calculated from the real part of the permittivity, to which a dc-conductivity makes no contribution, by an approximation of the Kramers–Kronig relation,[34]

$$\varepsilon''_{der}(\omega) = -\frac{\pi}{2}\frac{d\varepsilon'(\omega)}{d\ln\omega}. \tag{3}$$

This representation has proven especially useful to distinguish relaxational contributions by the eye, which are only slightly separated in frequency. This also holds true for the dielectric data of the mixture with 72 mol. % water in four different representations; see Fig. 6. Two different relaxation processes can be clearly distinguished in the conductivity free representation of the dielectric loss $\varepsilon''_{der}(\omega)$, whereas they are less obvious in the other representations.

In order to fit these dielectric spectra with model curves, we use an approach employed before on IL spectra,[28] where the faster process is described by the so-called MIGRATION model,[35] standing for MIsmatch Generated Relaxation for the Accommodation and Transport of IONs, and the slower process is described by a CD function [Eq. (1)].

The microscopic picture behind this approach is as follows: The CD function accounts for the reorientational motion of dipole moments. In the case of [BMIM][DCA], both the cation and the anion are equipped with a permanent dipole moment, but we expect that a single CD function is sufficient because the reorientational motions of cations and anions of similar size occur on similar timescales.[18,33]

The MIGRATION model accounts for the translational motion of the ions, i.e., the conductivity relaxation process via the following concept: When an ion performs a hop to a new site, mismatch is created between the ion's new position and the ionic neighborhood. There are two ways to reduce this mismatch: one is the single-particle-route, i.e., the ion hops backward to its original site, and second is the many-particle-route with the neighbors rearranging. The resulting differential equation for the correlation factor $W(t)$ is given by

$$-\dot{W}(t) = \omega_0\, W^2(t)\, \ln(W(t))[N_\infty + \ln(W(t))]^\lambda, \tag{4}$$

which when numerically solved and substituted in

$$\frac{\sigma^*(\omega)}{\sigma_0} = 1 + i\omega\int_0^\infty [W(t) - 1]\exp(-i\omega t)dt \tag{5}$$

gives the complex conductivity spectrum. Here, $\omega_0 = 1/\tau_\sigma$ marks the onset of dispersion, λ is a shape parameter, and N_∞ is the effective number of nearest neighbors of the central ion, which are not screened by other ions and are, therefore, available for the relaxation on the many-particle-route for $t \to \infty$.

The MIGRATION model in connection with a CD function for dipolar reorientation can describe the dielectric spectra in all representations quite well, both for the neat IL, as shown in Fig. 7, and for the mixture with 72 mol. % water, as shown in Fig. 6.

In Figs. 6 and 7, depolarized PCS data measured at the same temperature are added in the ε''_{der} representations. The peak in the light scattering susceptibility is located near the slow dielectric peak, indicating reorientational motion as its origin. While in the neat IL, the timescales of the BDS and the PCS process are identical for all temperatures, in the mixture, the timescales are slightly separated at high temperatures and approach each other at low temperatures. The latter behavior was also found in Ref. 32. The reason for this

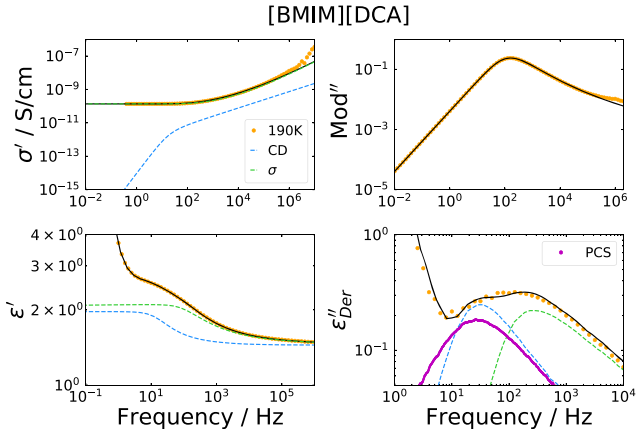

FIG. 7. Same as in Fig. 6 for the neat IL at 190 K.

behavior may be related to the fact that the reorientational correlation function probed by BDS is proportional to the first rank Legendre polynomial, while it is proportional to the second rank Legendre polynomial in PCS.[36] As a consequence, the ratio of the timescales is expected to obey the relation $1 \leq \frac{\tau_{BDS}}{\tau_{PCS}} \leq 3$ depending on the nature of the rotational mechanism,[37,38] which possibly changes upon cooling from rotational diffusion at high temperatures to large angle jumps on approaching the glass transition temperature. Additionally, the shape parameter β_{CD} of this process is identical in both experimental methods, which is not obvious in Figs. 6 and 7 because of the derivative representation of the BDS data, which distorts the apparent shape.

Qualitatively, however, the spectra do not change much from the neat IL to the mixture with 72 mol. % water. In particular, no third relaxational process appears, which could have been assigned to the reorientation of water molecules. This implies that the reorientational motions of cations, anions, and water occur on similar timescales in the studied mixture.

E. Small angle neutron scattering

Small angle neutron scattering (SANS) data were collected at 25 and at 5 °C, which almost lead to identical datasets, so we restrict our discussion to the 5 °C dataset, which is shown in Fig. 8. Four different mixtures of the deuterated IL with different amounts of D_2O were measured besides the neat IL, viz. 50, 72, 80, and 88 mol. %. D_2O was chosen to increase the scattering contrast between the mostly protonated cation and deuterated water. A structural peak shows up in the data for all water concentrations in a q-range from ~0.3 to 0.6 Å^{-1}, located at increasing q-values from high water concentrations to the neat IL. Such a peak in SANS spectra was previously interpreted as evidence for the existence of water pockets in a [BMIM][NO_3]-water mixture;[5] however, the scattering data of the neat IL were not shown in this work. In the present system, the neat IL also exhibits a structural peak, which, of course, is not surprising since nanostructuration is known for long times to occur in neat ILs.[12,39] This means the mere existence of a structural peak in this q-range in SANS measurements of IL–water mixtures is not sufficient to prove the existence of water pockets.

To analyze the SANS data, we apply a core–shell model, where the following assumptions were made: The spherical core consists of anions in the neat IL and anions and D_2O in the 50 mol. % mixtures. The core is surrounded by cations, which form the spherical shell of this model. We used the following scattering length densities (SLDs): $SLD_{anion} = 4.0 \times 10^{-6}$ Å^{-2}, $SLD_{cation} = 1.2 \times 10^{-6}$ Å^{-2}, and $SLD_{D_2O} = 6.3 \times 10^{-6}$ Å^{-2}. For higher water concentrations, the spherical core–shell model was no longer able to describe the data. We therefore used an elliptical core–shell model with D_2O in the core, surrounded by a shell of anions + cations. In all cases, the SLD of the solvent was determined by assuming a mixture of IL + D_2O.

This model fits the data quite well, and some reasonable tendencies can be observed, in particular, a change from a globular to an ellipsoidal shape of the core–shell structure between 50 and 72 mol. %, i.e., in the same water concentration region where the DDAA peak appears in the Raman spectra. Interestingly, at 50 mol. %, the SANS scattering pattern is almost identical to that of neat IL. It may indicate that the water pockets do not exist at 50 mol. % concentration of D_2O. At higher concentrations of D_2O (72%–88%), the average size of the core–shell structures increases, indicating that the water tends to localize in larger structures. For example, at 72 mol. % D_2O, the size of the structure is ~2 nm across on the long axis of the ellipsoid, which is for the mixture in accordance with similar water pocket sizes.[5] However, we emphasize that this model should not be over-interpreted. First, rather different models were already successfully used to fit similar data,[6,40] and

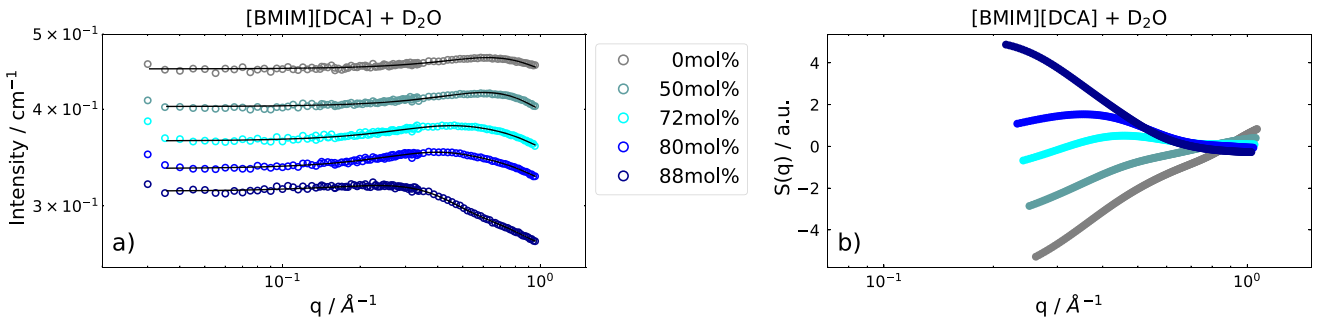

FIG. 8. (a) SANS spectra at 5 °C for different D_2O concentrations as indicated. The solid lines represent fits with a core–shell model; see the text for details. (b) Full structure factor from MD simulations for different water concentrations, highlighting the qualitative similarity with the SANS data.

second, the present core–shell model leads to a rather unlikely description of the neat IL with a clustering of anions in a spherical core. In the latter case, the structural peak arises more likely due to the alternation of polar and apolar domains.[41]

In particular, we aim at a more qualitative picture from these SANS measurements rather than focusing on the model parameters: In the neat IL, a structural peak arises most probably due to the high scattering length density of the anions, which are spaced by the apolar butyl groups of the cations. By the addition of deuterated water, these structures swell because water tends to accumulate near the anions. In the following, we qualitatively compare this picture with the findings from MD simulations.

F. Molecular dynamics simulation

We compute the neutron scattering structure factor $S(q)$ from the atomic positions in our MD simulations for comparison with the experimental data. The starting point is given by

$$S(q) = \frac{\sum_{i=1}^{N}\sum_{j=1}^{N} x_i x_j b_i b_j H_{ij}(q)}{\left(\sum_{i=1}^{N} x_i b_i\right)^2} \tag{6}$$

with the mole fractions $x_{i,j}$ of atom types i or j and the corresponding neutron scattering lengths $b_{i,j}$.[42] The partial structure factor $H_{ij}(q)$ is given by the Fourier transformation of the radial distribution function $g_{ij}(r)$,

$$H_{ij}(q) = 4\pi\rho_0 \int_0^{r_{\max}} r^2 (g_{ij}(r) - 1)\frac{\sin(qr)}{qr}\mathrm{d}r, \tag{7}$$

where ρ_0 stands for the average number density of all atoms and $r_{\max}$ stands for the maximum distance for the $g_{ij}(r)$ calculation, which is given by half the box length L. This limits the accessible q-range to $q \geq 4\pi/L$. Since we did not perform simulations with heavy water, we consider the hydrogens of the water molecules as deuterons to obtain $S(q)$ that can be compared to experimental data.

The calculated structure factors for the different water concentrations are shown in Fig. 8(b). It can be seen that a shoulder shows up for the neat IL at around 0.6 Å^{-1}. By increasing the water concentration, this shoulder develops into a clear peak, which shifts to lower scattering vector values for higher water concentrations, very similar to the experimental observations by SANS shown in Fig. 8(a). Together with observations from visual inspection of representative snapshots of the simulated system (see Fig. 14 in the Appendix for an exemplary configuration), this supports the picture that water accumulates near the anions and thus swells the nanostructure inherent to the neat IL, as put forward in Sec. III E.

In order to further elucidate the number of water molecules in water clusters, we determined the latter using a simple geometric criterion: Two water molecules are part of the same cluster if their O–O distance is no larger than 0.35 nm [corresponding to the first minimum in the O–O pair distribution function $g(r)$ of pure water]. The probability of a water molecule to be in a cluster comprised of n molecules is shown in Fig. 9 for water concentrations of 50, 72, and 80 mol. %. The vertical lines indicate the total amount of water molecules in the respective mixture. It can be seen that for

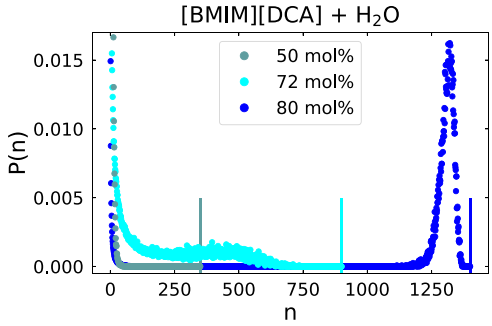

FIG. 9. Probability of a water molecule to be located in a water cluster of size n calculated from MD simulations for different water concentrations. The vertical lines indicate the total amount of water molecules in the respective mixture.

the case of 50 mol. %, all water molecules are located in very small clusters. In contrast, for the 80 mol. % mixture, most molecules are in a very large cluster of a size nearly equal to the total number of water molecules in the simulation box. This means that a continuous water phase has formed, spanning the whole simulation box. We mention that the cluster size in the case of a percolating network will depend on the size of the simulation box. In between these two concentrations, at 72 mol. % water, a very broad distribution of cluster sizes is found, with a hump around 450 water molecules per cluster. This finding supports the results from Raman spectroscopy, where it was found that at these concentrations, large water clusters occur as evidenced by the *DDAA* peak.

G. Nuclear magnetic resonance

To obtain cation self-diffusion coefficients of the 72 mol. % water–IL mixture and the pure IL, we performed ^{1}H SFG NMR measurements, where a magnetic field with a static gradient g along the z axis is applied. Under these circumstances, the Larmor frequency of a nuclear spin depends on its position $\omega_L(z) = -\gamma B(z)$, with γ being the gyromagnetic ratio of the observed nucleus and $B(z) = B_0 + \gamma z$. Hence, molecular diffusion results in frequency changes, which can be observed utilizing a stimulated-echo (STE) pulse sequence: $90°$–t_e–$90°$–t_m–$90°$–t_e. The two evolution times t_e serve to encode the respective resonance frequencies, while the mixing time t_m allows for diffusion in the meantime. The measured STE signals decay due to free diffusion according to[43,44]

$$S(t_m, t_e) \propto \exp\left[-q^2 D\left(t_m + \frac{2}{3}t_e\right)\right]. \tag{8}$$

Here, D is the diffusion coefficient and $q = \gamma g t_e$ can be considered as a generalized scattering vector, which determines the inverse length scale of the experiment and amounts typically to $q^{-1} \approx 1\ \mu$m for NMR diffusometry. In the present measurements, we record SFG STE decays for several fixed evolution times t_e as a function of the mixing time t_m at each temperature and globally fit these data to Eq. (8) using a single value of D.

The diffusion constants of the cation in the mixture with 72 mol. % water from NMR measurements are shown in Fig. 10

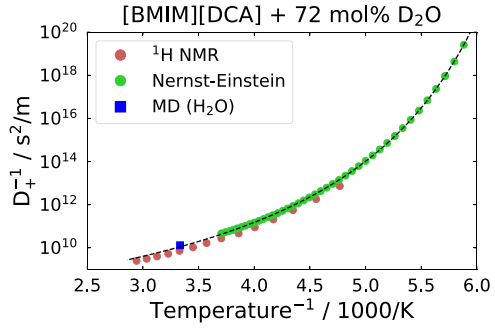

FIG. 10. Inverse diffusion constants of the cation in the mixture with 72 mol. % water from SFG NMR measurements and calculated via the Nernst–Einstein equation from conductivity measurements. The differences between the two techniques are ascribed to ion correlations and expressed by a Haven ratio larger than unity. In addition, the MD simulation result at 300 K is included.

and compared to values calculated via the Nernst–Einstein (NE) equation

$$\sigma_0 = \frac{e^2}{k_B T}\left(N_+ z_+^2 D_+ + N_- z_-^2 D_-\right), \tag{9}$$

using the dc-conductivity values σ_0 from dielectric spectroscopy measurements. In Eq. (9), the number density of the cation N_+ equals the one of the anion N_-. The same holds true for the squared charges $z_\pm^2$. The diffusion constant of the anion D_- is related to that of the cation D_+ based on the MD simulation result $D_- = 1.64 D_+$ for the 72 mol. % mixture. This ratio was assumed to hold for all temperatures. In passing, we note that the cation diffusion coefficients from the SFG and MD studies are in good agreement, indicating that the used model is capable of reproducing not only structural but also dynamical properties of the studied IL–water mixtures.

As can be seen, the data from NMR measurements overlap with those calculated from the NE equation in a temperature range of 40 K. We find that the temperature dependence is very similar, but the values are not identical. This behavior is well known for neat ILs (see, for example Ref. 45, and references therein) and can be quantified through the Haven ratio

$$H = \frac{D_{\mathrm{NMR}}}{D_{\mathrm{NE}}}. \tag{10}$$

In our case, $H > 1$, indicating that the ion diffusion is faster than the charge transport. The microscopic origin of this effect is still highly debated, explanations aiming at ion pairing, i.e., neutral ion pairs that do not contribute to conductivity,[46] or cross correlations in the current autocorrelation function,[47,48] or charge transfer leading to non-integer charges of the ions.[45] Irrespective of the exact microscopic origin, it is noteworthy that the largely temperature independent Haven ratio of $H = 1.69 \pm^{0.26}_{0.12}$ for the mixture with 72 mol. % water is similar to the value of $H = 1.99$ for the neat IL at the highest temperature in the overlap region, which, however, increases up to 2.96 at the lowest temperature.

This means that the mixture cannot be regarded as a dilute electrolyte, for which the Haven ratio would equal unity. Instead, the interactions of the ions, resulting in ion-pair formation, cross correlations in the current autocorrelation functions, or charge transfer, are of similar strength in the mixture as in the neat IL.

IV. DISCUSSION

By combining all the above findings from experiments and simulations, a clear picture of the structure and the IL dynamics of the mixture of [BMIM][DCA] with water emerges: The neat IL is nanostructured, as evidenced by SANS measurements, most probably due to the polar groups being separated from each other by the nonpolar alkyl tails, as found for a wide variety of ILs. When adding small amounts of water, the H_2O molecules tend to be incorporated into polar regions; more precisely, they form H-bonds with the anions, as shown by Raman spectroscopy. Up to water concentrations of 50 mol. %, only individual or very few water molecules are located in a single polar domain, as evidenced by the absence of the *DDAA*-Raman band, which is assigned to fully bonded water, and by the water cluster sizes from simulations.

From 60 mol. % water upward, the *DDAA*-Raman band shows up and intensifies, which is evident for the presence of fully bonded water in these mixture. As can be seen from the cluster size calculation, at 72 mol. %, a broad distribution of the number of water molecules located in one cluster shows up. At the same concentration, the peak in the SANS spectrum shifts to lower values of q, indicating an increasing size of the nanostructures, and a comparison with the structure factor of water from simulations shows that, indeed, water clustering takes place on these length scales. This means that in the 72 mol. % mixture, nanoscale water clusters, or "water pockets," are present, which do not crystallize upon supercooling as seen by DSC measurements, where no freezing or melting peaks were detected. Also in the light scattering cell with sample volumes of 2–3 ml and measurement times spanning several days at low temperatures, no crystallization was observed.

This means that not only the nanoscale water clusters in the IL matrix do not crystallize but also the whole sample stays amorphous over the whole temperature range from above room temperature down to the glass transition temperature. Moreover, the mixture behaves like a regular glass former in all respects, as can be seen, for example, in Fig. 11, where the correlation times obtained from DLS, BDS, and DSC are shown. The solid line represents a fit to the DLS data with a Vogel–Fulcher–Tammann equation (VFT),

$$\tau = \tau_0 \exp\left(\frac{E}{T - T_0}\right), \tag{11}$$

which is commonly used to describe the temperature dependence of correlation times or viscosities of glass forming liquids.

It can be clearly seen that all rotational correlation times agree, indicating that the molecular motions probed by DLS and BDS are connected to the glass transition as probed by DSC. Moreover, no decoupling between translational and rotational motions occurs. This can be inferred from the fact that the hopping correlation times from the MIGRATION model and the diffusion correlation times calculated from the SFG data using the Stokes–Einstein–Debye relation [SED, Eq. (12)] show the same temperature dependence as the BDS and PCS rotational correlation times,

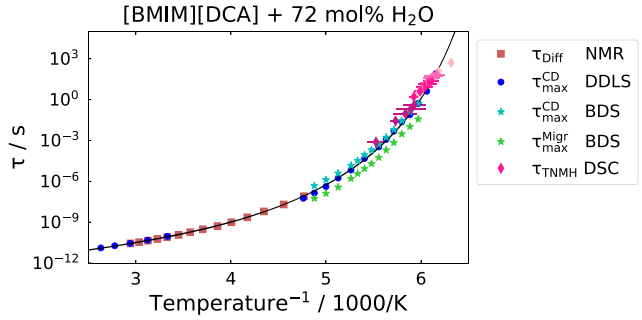

FIG. 11. Correlation times taken at the peak maximum $\tau = 1/\omega_{max}$ from dielectric spectroscopy and light scattering. Time constants from DSC measurement are calculated with the TNMH model, and time constants from NMR measurements for the mixture with D_2O were determined with the SED equation. The solid line represents a VFT fit to the time constants from light scattering.

$$\tau_{\mathrm{diff}} = \frac{2}{9\, D_{\mathrm{NMR}}} R_h^2. \tag{12}$$

The value of the hydrodynamic radius R_h = 2.23 Å is chosen in such a way that the correlations times τ_{diff} coincide with the ones from light scattering. Furthermore, the mixture cannot be regarded as a dilute electrolyte as can be seen from the comparison of diffusion constants from NMR and dielectric measurements, where the Haven ratio is markedly larger than unity, indicating strong ion correlations.

We were not able to detect the dynamics of water molecules in the mixture with dielectric spectroscopy and light scattering; our focus was thus on the dynamics of the ions. Therefore, as a next step, further investigations are under way to probe the dynamics of supercooled water in the presented systems using ^{17}O NMR and quasi-elastic neutron scattering.

V. CONCLUSION

We used a combination of various experimental techniques and MD simulations to investigate mixtures of the ionic liquid [BMIM][DCA] with water. It turned out that a combination of several techniques is required to clarify the existence of nanoscale water domains in the mixtures, the so-called water pockets. We presented evidence that nanoscale water clusters are present in a small concentration range from ~60 to 72 mol. % water. Below this range, single or only a few water molecules are located near the anions, whereas at higher water concentrations, a percolating water network emerges spanning the whole sample. We showed, furthermore, that the mixture of 72 mol. % water behaves like a common glass former, and neither the water nor the IL matrix crystallizes, opening up the possibility to investigate supercooled nanoscale water clusters in a fully amorphous and soft IL matrix.

ACKNOWLEDGMENTS

Financial support from the Deutsche Forschungsgemeinschaft (DFG) under Grant No. BL1192/3 is gratefully acknowledged.

AUTHOR DECLARATIONS

Conflict of Interest

There are no conflicts of interest to disclose.

DATA AVAILABILITY

The data that support the findings of this study are available from the corresponding author upon reasonable request

APPENDIX: RAMAN FITTING PARAMETERS AND MD SNAPSHOT

In Fig. 12, the fit parameters of the fits to the Raman spectra of the IL–water mixtures with different water concentrations as shown in Fig. 4 are shown, where $\Delta\nu_{\mathrm{shift}}$ is the frequency shift of the respective subband of the mixture in comparison to neat water, as shown in Fig. 3. FWHM is the full width at half maximum, and Int. is the intensity of the different subbands. The frequency shift of the DDAA band is discussed in the main text, and the other bands are fixed at their positions for neat water. The intensity naturally increases upon the addition of water, and so does the FWHM of the DDAA and DA subbands.

The C–N stretching region of the anion from Raman measurements is shown in Fig. 13 for different water concentrations. One can

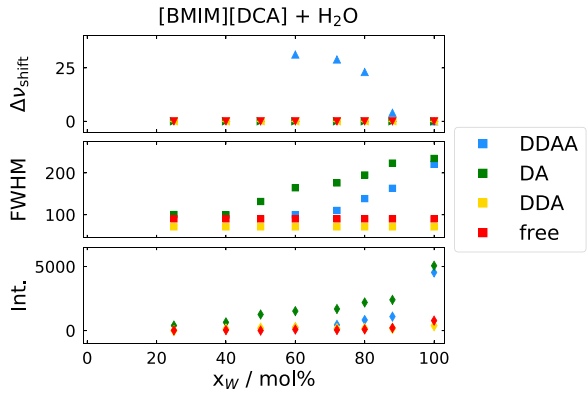

FIG. 12. Fit parameters of the fits to the Raman spectra of the IL–water mixtures.

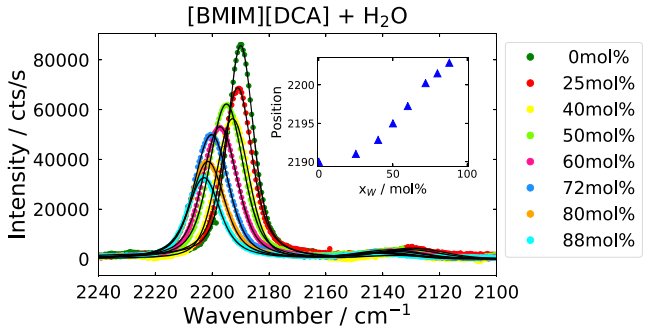

FIG. 13. Raman spectrum in the C–N stretching region of the anion for mixtures of IL with water as indicated. The inset shows the blue shift of this vibration with increasing water content.

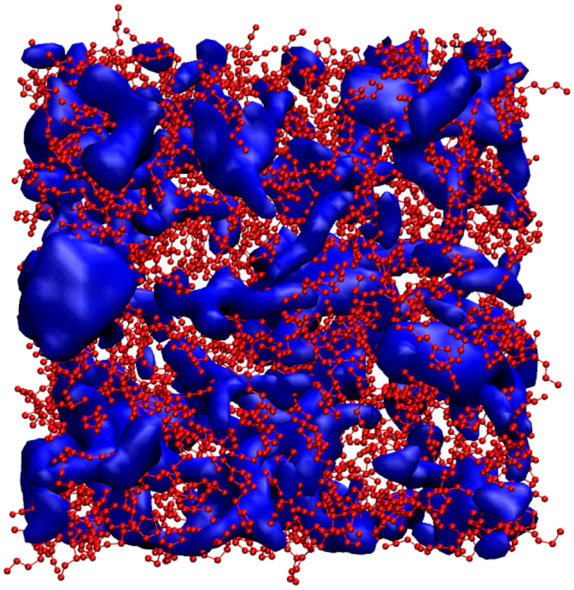

FIG. 14. Snapshot of the molecular dynamic simulation with a water concentration of 72 mol. %. Ions are marked in red, and water is marked in blue.

see that the peak position is blue shifted upon the addition of water, indicating the increasing strength of the C–N bond, as discussed in more detail in the main text.

In Fig. 14, a snapshot from the molecular dynamics simulation of the mixture with 72 mol. % water is shown, where one can see the clustering of the water shown in blue between the ions in red.

REFERENCES

[1] J. Jacquemin, P. Husson, A. A. H. Padua, and V. Majer, "Density and viscosity of several pure and water-saturated ionic liquids," Green Chem. **8**(2), 172–180 (2006).

[2] P. Sippel, V. Dietrich, D. Reuter, M. Aumüller, P. Lunkenheimer, A. Loidl *et al.*, "Impact of water on the charge transport of a glass-forming ionic liquid," J. Mol. Liq. **223**, 635–642 (2016).

[3] O. Palumbo, F. Trequattrini, J.-B. Brubach, P. Roy, and A. Paolone, "Crystallization of mixtures of hydrophilic ionic liquids and water: Evidence of microscopic inhomogeneities," J. Colloid Interface Sci. **552**, 43–50 (2019).

[4] J. Vila, P. Gines, E. Rilo, O. Cabeza, and L. Varela, "Great increase of the electrical conductivity of ionic liquids in aqueous solutions," Fluid Phase Equilib. **247**(1–2), 32–39 (2006).

[5] H. Abe, T. Takekiyo, M. Shigemi, Y. Yoshimura, S. Tsuge, T. Hanasaki *et al.*, "Direct evidence of confined water in room-temperature ionic liquids by complementary use of small-angle X-ray and neutron scattering," J. Phys. Chem. Lett. **5**(7), 1175–1180 (2014).

[6] J. Gao and N. J. Wagner, "Water nanocluster formation in the ionic liquid 1-butyl-3-methylimidazolium tetrafluoroborate ($[C_4mim][BF_4]$)–D_2O mixtures," Langmuir **32**(20), 5078–5084 (2016).

[7] B. Fazio, A. Triolo, and G. Di Marco, "Local organization of water and its effect on the structural heterogeneities in room-temperature ionic liquid/H_2O mixtures," J. Raman Spectrosc. **39**(2), 233–237 (2008).

[8] J. Kausteklis, M. Talaikis, V. Aleksa, and V. Balevičius, "Raman spectroscopy study of water confinement in ionic liquid 1-butyl-3-methylimidzolium nitrate," J. Mol. Liq. **271**, 747–755 (2018).

[9] K. Saihara, Y. Yoshimura, S. Ohta, and A. Shimizu, "Properties of water confined in ionic liquids," Sci. Rep. **5**(1), 10619 (2015).

[10] M. H. Kowsari and S. M. Torabi, "Molecular dynamics insights into the nanoscale structural organization and local interaction of aqueous solutions of ionic liquid 1-butyl-3-methylimidazolium nitrate," J. Phys. Chem. B **124**(32), 6972–6985 (2020).

[11] A. Verma, J. P. Stoppelman, and J. G. McDaniel, "Tuning water networks via ionic liquid/water mixtures," Int. J. Mol. Sci. **21**(2), 403 (2020).

[12] A. Triolo, O. Russina, H.-J. Bleif, and E. Di Cola, "Nanoscale segregation in room temperature ionic liquids," J. Phys. Chem. B **111**(18), 4641–4644 (2007).

[13] S. Cerveny, F. Mallamace, J. Swenson, M. Vogel, and L. Xu, "Confined water as model of supercooled water," Chem. Rev. **116**(13), 7608–7625 (2016).

[14] M. Y. Ivanov, S. A. Prikhod'ko, N. Y. Adonin, and M. V. Fedin, "Structural anomalies in binary mixtures of ionic liquid [Bmim] BF_4 with water studied by EPR," J. Phys. Chem. B **123**(46), 9956–9962 (2019).

[15] H. Abe, T. Yamada, and K. Shibata, "Dynamic properties of nano-confined water in an ionic liquid," J. Mol. Liq. **264**, 54–57 (2018).

[16] M. Klähn, C. Stüber, A. Seduraman, and P. Wu, "What determines the miscibility of ionic liquids with water? Identification of the underlying factors to enable a straightforward prediction," J. Phys. Chem. B **114**(8), 2856–2868 (2010).

[17] E. P. Grishina, L. M. Ramenskaya, N. O. Kudryakova, K. V. Vagin, A. S. Kraev, and A. V. Agafonov, "Composite nanomaterials based on 1-butyl-3-methylimidazolium dicianamide and clays," J. Mater. Res. Technol. **8**(5), 4387–4398 (2019).

[18] M. Becher, E. Steinrücken, and M. Vogel, J. Chem. Phys. **151**, 194503 (2019).

[19] E. Steinrücken, M. Becher, and M. Vogel, J. Chem. Phys. **153**, 104507 (2020).

[20] R. Giernoth and D. Bankmann, "Transition-metal free ring deuteration of imidazolium ionic liquid cations," Tetrahedron Lett. **47**(25), 4293–4296 (2006).

[21] B. Geil, "Measurements of translational molecular diffusion using ultra-high magnetic field gradient NMR," Concepts Magn. Reson. **10**, 299–321 (1998).

[22] H. J. C. Berendsen, D. van der Spoel, and R. van Drunen, "GROMACS: A message-passing parallel molecular dynamics implementation," Comput. Phys. Commun. **91**, 43–56 (1995).

[23] M. J. Abraham, T. Murtola, R. Schulz, S. Páll, J. C. Smith, B. Hess *et al.*, "GROMACS: High performance molecular simulations through multi-level parallelism from laptops to supercomputers," SoftwareX **1-2**, 19–25 (2015).

[24] G. Bussi, D. Donadio, and M. Parrinello, "Canonical sampling through velocity rescaling," J. Chem. Phys. **126**, 014101 (2007).

[25] B. Doherty, X. Zhong, S. Gathiaka, B. Li, and O. Acevedo, "Revisiting OPLS force field parameters for ionic liquid simulations," J. Chem. Theory Comput. **13**, 6131–6145 (2017).

[26] J. L. F. Abascal and C. Vega, "A general purpose model for the condensed phases of water: TIP4P/2005," J. Chem. Phys. **123**, 234505 (2005).

[27] T. Darden, D. York, and L. Pedersen, "Particle mesh Ewald: An *N* log(*N*) method for Ewald sums in large systems," J. Chem. Phys. **98**, 10089 (1993).

[28] F. Pabst, Z. Wojnarowska, M. Paluch, and T. Blochowicz, "On the temperature and pressure dependence of dielectric relaxation processes in ionic liquids," Phys. Chem. Chem. Phys. **23**, 14260–14275 (2021).

[29] Q. Sun, "The Raman OH stretching bands of liquid water," Vib. Spectrosc. **51**(2), 213–217 (2009).

[30] S. J. Brotton, M. Lucas, T. N. Jensen, S. L. Anderson, and R. I. Kaiser, "Spectroscopic study on the intermediates and reaction rates in the oxidation of levitated droplets of energetic ionic liquids by nitrogen dioxide," J. Phys. Chem. A **122**(37), 7351–7377 (2018).

[31] V. H. Paschoal, L. F. O. Faria, and M. C. C. Ribeiro, "Vibrational spectroscopy of ionic liquids," Chem. Rev. **117**(10), 7053–7112 (2017).

[32] F. Pabst, J. Gabriel, P. Weigl, and T. Blochowicz, "Molecular dynamics of supercooled ionic liquids studied by light scattering and dielectric spectroscopy," Chem. Phys. **494**, 103–110 (2017).

[33]F. Pabst, J. Gabriel, and T. Blochowicz, "Mesoscale aggregates and dynamic asymmetry in ionic liquids: Evidence from depolarized dynamic light scattering," J. Phys. Chem. Lett. **10**(9), 2130–2134 (2019).
[34]M. Wübbenhorst and J. van Turnhout, "Analysis of complex dielectric spectra. I. One-dimensional derivative techniques and three-dimensional modelling," J. Non-Cryst. Solids **305**(1–3), 40–49 (2002).
[35]K. Funke, R. D. Banhatti, D. M. Laughman, L. G. Badr, M. Mutke, A. Santic *et al.*, "First and second universalities: Expeditions towards and beyond," Z. Phys. Chem. **224**(10–12), 1891–1950 (2010).
[36]B. J. Berne and R. Pecora, *Dynamic Light Scattering: With Applications to Chemistry, Biology, and Physics*, Dover Books on Physics Series (Dover Publications, 1976).
[37]E. Ivanov, "Theory of rotational Brownian motion," Sov. Phys. JETP **18**, 1041–1045 (1964).
[38]A. Brodin and E. A. Rössler, "Depolarized light scattering study of glycerol," Eur. Phys. J. B **44**(1), 3–14 (2005).
[39]R. Hayes, G. G. Warr, and R. Atkin, "Structure and nanostructure in ionic liquids," Chem. Rev. **115**(13), 6357–6426 (2015).
[40]C. P. Cabry, L. D'Andrea, K. Shimizu, I. Grillo, P. Li, S. Rogers *et al.*, "Exploring the bulk-phase structure of ionic liquid mixtures using small-angle neutron scattering," Faraday Discuss. **206**, 265–289 (2017).
[41]J. J. Hettige, H. K. Kashyap, H. V. R. Annapureddy, and C. J. Margulis, "Anions, the reporters of structure in ionic liquids," J. Phys. Chem. Lett. **4**(1), 105–110 (2013).
[42]V. F. Sears, "Neutron scattering lengths and cross sections," Neutron News **3**(3), 26–37 (1992).
[43]P. T. Callaghan, *Principles of Nuclear Magnetic Resonance Microscopy* (Clarendon Press, Oxford, 1991).
[44]R. Kimmich, *NMR: Tomography, Diffusometry, Relaxometry* (Springer, Berlin, 1997).
[45]F. Philippi, D. Rauber, M. Springborg, and R. Hempelmann, "Density functional theory descriptors for ionic liquids and the charge-transfer interpretation of the Haven ratio," J. Phys. Chem. A **123**(4), 851–861 (2019).
[46]K. Ueno, H. Tokuda, and M. Watanabe, "Ionicity in ionic liquids: Correlation with ionic structure and physicochemical properties," Phys. Chem. Chem. Phys. **12**(8), 1649–1658 (2010).
[47]J. C. Dyre, P. Maass, B. Roling, and D. L. Sidebottom, "Fundamental questions relating to ion conduction in disordered solids," Rep. Prog. Phys. **72**(4), 046501 (2009).
[48]K. R. Harris, "Relations between the fractional Stokes–Einstein and Nernst–Einstein equations and velocity correlation coefficients in ionic liquids and molten salts," J. Phys. Chem. B **114**(29), 9572–9577 (2010).